Polymer 190 (2020) 122248

Contents lists available at ScienceDirect

Polymer

journal homepage: http://www.elsevier.com/locate/polymer

Alendronate-functionalized poly(amido amine) cryogels of high-toughness for biomedical applications

Melek Naz Guven [a], Gozde Demirci [b], Seckin Altuncu [a], Umit Gulyuz [c,d], Oguz Okay [c], Havva Yagci Acar [b], Duygu Avci [a,*]

[a] Department of Chemistry, Bogazici University, 34342, Bebek, Istanbul, Turkey
[b] Department of Chemistry, Koc University, 34450, Sariyer, Istanbul, Turkey
[c] Department of Chemistry, Istanbul Technical University, Maslak, 34469, Istanbul, Turkey
[d] Department of Chemistry and Chemical Processing Technologies, Kirklareli University, Luleburgaz, 39750, Kirklareli, Turkey

ARTICLE INFO

Keywords:
Macromers
Alendronate
Poly(amido amine)s

ABSTRACT

Novel bisphosphonic acid-functionalized poly(amido amine) (PAA) macromers were synthesized through aza-Michael addition of sodium alendronate (ALE) and 5-amino-1-pentanol (AP) to N,N′-methylene bisacrylamide at two different molar ratios, with macromer only having AP as comparison control. The macromers were photopolymerized to cryogels whose swelling, biodegradation and mineralization properties were studied. Biodegradation was most strongly affected by the macromer molecular weight. In mineralization studies, the control cryogel nucleated HAP, the others another type of biological apatite; the extent of mineralization depending on ALE concentration. Cryogel-apatite composites were studied by SEM, FTIR, XRD and thermogravimetric analysis. Mechanical tests reveal compressions up to 97% for cryogels, showing their high toughness. Young's modulus and compressive fracture stress increase with ALE content to 10 kPa and 2.2 ± 0.4 MPa, respectively. The modulus increased significantly in mineralization due Ca^{2+}-ALE bindings forming physical cross-links. Degradation products of ALE-containing cryogels showed dose, composition and cell type dependent cytotoxicity when incubated with osteosarcoma cells lines, Saos-2 and U-2 OS, and healthy C2C12 muscle cells.

1. Introduction

Hydrogels, water-swollen 3D hydrophilic polymer networks, possess unique properties making them suitable for many biomedical applications [1]. They have been intensively researched for tissue engineering, regenerative medicine and delivery of theranostic agents, etc. [2,3]. Some hydrogels can be designed to respond to external stimuli such as pH, temperature and redox state [4–7]. The nanoscale mesh size of homogeneous hydrogels can facilitate the access of nutrients and oxygen, the drain of metabolites, and hence, may provide a temporary scaffold to guide the ingrowth of vascular and neural tissues. Yet, the nano-sized scale of the network of hydrogels precludes certain applications requiring incorporation, growth, or support of larger-scale bio-objects, e.g. plasmids, viruses, cell organelles and in particular, cells. Cryogels, a class of gels prepared via cryopolymerization, can address this need: They feature a micro-scale macroporous network, and possess higher elasticity, toughness, and flexibility as compared to the nanoporous hydrogels [8–12]. These properties enable a wide range of applications for cryogels in the biotechnology, bioseparation and biomedicine fields featuring e.g. purification and immobilization of proteins, nucleic acids, and polysaccharides [13]; separations of whole cells, environmental separations and even or heavy metal removal; tissue engineering applications. The cryopolymerization procedure to form a cryogel involves polymerization of precursors dissolved in the unfrozen portion of a suitable solvent (such as water) around the interconnected ice crystals of the frozen portion. After the polymerization is completed, the frozen mixture is brought to room temperature, melting the ice crystals to give the porous cryogel. The shape, size and degree of interconnection of the pores depend on many factors such as monomer concentration and polymerization temperature; but the pores are generally larger than those of hydrogels, can be up to 200 mm for the so-called supermacropores [14].

Poly(amido amine)s (PAAs) are a class of synthetic polymers mainly obtained by Michael-type polyaddition of primary amines or bissecondary amines to bisacrylamides [15–17]. They have biomedically important properties such as biocompatibility, biodegradability and

* Corresponding author.
E-mail address: avcid@boun.edu.tr (D. Avci).

https://doi.org/10.1016/j.polymer.2020.122248
Received 22 November 2019; Received in revised form 28 January 2020; Accepted 1 February 2020
Available online 3 February 2020

non-toxicity. Synthetic flexibility of the polymerization reaction by using different bisacrylamides and amines enables incorporation of additional functionalities such as side chain substituents. PAA hydrogels functionalized with bioactive and biomimetic compounds can be designed as scaffolds for tissue engineering. For example, incorporation of agmatine unit (RGD mimicking structure) to PAA hydrogels results in an enhancement of cell adhesion [18–22]. Amphoteric PAAs with both amine and carboxylate groups are protein-like in some sense [23]. Copolymerization of acrylamide-terminated PAA oligomers with 2-hydroxyethyl methacrylate, polyethylene glycol diacrylate, or N-isopropyl acrylamide leads to hydrogels with tunable degradation rate and mechanical properties [24–26]. A tissue adhesive was designed using catechol-containing PAA crosslinked by the Fe^{3+} ion [27].

Hydrogels containing functional groups such as phosphate, phosphonate, bisphosphonate, carboxylate, sulfonate, and hydroxyl are known to serve as organic templates within which hydroxyapatite (HAP, $Ca_{10}(PO_4)_6(OH)_2$) crystals can be synthesized; in a way similar to the natural bone [28–32]. Bisphosphonates (BPs) are structural analogues of naturally existing pyrophosphate with increased chemical and enzymatic stability. They have strong affinity for the bone mineral HAP, enabling them to chelate calcium ions and to prevent bone dissolution [33]. Therefore, there is a growing interest in the use of BPs in combination with scaffolds for bone tissue engineering [34–42]. Phosphate, phosphonate and BP groups on materials surfaces lead to improved affinity of the materials for osteoblast-like cells [43,44]. Four PAA conjugates containing BP have already been reported in the literature. Neridronic acid (0.9–3.74 wt%) was incorporated into PAA by a one-pot aqueous phase Michael addition reaction of N,N′-methylene bisacrylamide with amines [45]. Similarly, PAA conjugates containing another BP and curcumin were synthesized via a one-pot aqueous phase Michael addition reaction [46]. Both conjugates yielded linear polymers, and were evaluated for potential drug-delivery systems. In another work, neridronate and pamidronate-functionalized PAA oligomers were found to be good candidates to be used in long-term therapy for bone resorption, increasing poor absorptivity of the BPs [47].

In this study we report, for the first time to our knowledge, synthesis of PAA macromers functionalized with alendronate as a BP, and their cryogels for potential bone tissue scaffold applications. We also investigate the effects of the macromer structure as well as BP content on the cryogel properties. We use two different alendronate concentrations to highlight the effect of BP functionalization on the swelling, degradation, mineralization, and mechanical properties of the cryogels. As will be seen below, both the molecular weight of PAA precursors and their BP contents significantly affect the swelling, thermal, and degradation behavior of the resulting cryogels. A significant mechanical performance improvement was observed after their mineralization due to the formation of ionic bonds acting as additional cross-links.

2. Materials and methods

2.1. Materials

N,N′-methylene bisacrylamide, 5-amino-1-pentanol, 2-hydroxy-4′-(2-hydroxyethoxy)-2-methylpropiophenone (Irgacure 2959) and all solvents were purchased from Sigma-Aldrich and used as received. Phosphate buffered saline (PBS) was obtained from Biomatik Corporation (Canada). Sodium alendronate (ALE) was a kind gift from DEVA A.Ş. Dulbecco's Modified Eagle Medium (DMEM) (with L-glutamine and high glucose (4.5 g/l)), penicillin/streptomycin (pen-strep), fetal bovine serum (FBS) and trypsin-EDTA were purchased from Diagnovum, Ebsdorfergrund (Germany). Thiazolyl blue tetrazolium bromide (MTT) was provided Gold Biotechnology (USA) and phosphate buffered saline (PBS) tablets was obtained from BBI Life Sciences (China). 96-Well plates were purchased from Nest Biotechnology (China). Saos-2 human osteosarcoma cells were a kind gift of Dr. Halil Kavakli (Department of Molecular Biology and Genetics, Koc University, Istanbul, Turkey). U-2 OS human bone osteosarcoma epithelial cells were a kind gift of Prof. Devrim Gozuacık (Department of Molecular Biology, Genetics and Bioengineering, Sabancı University, Istanbul, Turkey). C2C12 mouse myoblast muscle cells were obtained from ATCC, Manassas (USA).

2.2. Methods

The chemical structures of PAA macromers were confirmed by ^{1}H NMR and FTIR spectroscopies. ^{1}H NMR spectra were recorded on a Varian Gemini 400 MHz spectrometer using D_2O as solvent. FTIR spectra were collected between 400 cm^{-1} and 4000 cm^{-1} by a Thermo Scientific Nicolet 380 spectrometer. Potentiometric titrations of macromers were carried out using a WTW Inolab 720 pH meter and WTW SenTix 41 epoxy pH electrode at room temperature. Differential scanning calorimetry (DSC) (TA Instruments Q100) was used to determine the glass transition temperatures (T_g) of the macromers. All samples (5–10 mg) were sealed in aluminium pans and heated under nitrogen atmosphere from −80 °C to 80 °C with a scanning rate of 10 °C min^{-1}. The morphologies of the cryogel samples were examined with scanning electron microscopy (SEM) (FEI-Philips XL30) with an accelerating voltage of 10.0 kV. The lyophilized hydrogel samples were sputter coated with a platinum layer and their internal fracture surface was examined. The X– ray powder diffraction (XRD) analysis (Rigaku-D/MAX-Ultima diffractometer) was used to identify the mineral phase of materials. Degradation studies were done using an incubator shaker (VWR) operating at 37 °C and 200 rpm. The mineral content of the cryogels was determined from thermogravimetric measurements (TGA). TGA studies were performed using a PerkinElmer STA 6000 machine. Samples were heated up to 700 °C at a rate of 10 °C min^{-1} under nitrogen atmosphere.

2.3. Synthesis of PAA macromers

PAA macromers were synthesized from N,N′-methylene bisacrylamide (MBA), 5-amino-1-pentanol (AP) and sodium alendronate (ALE) at a total concentration of 0.4 M in water/methanol mixture (v/v = 1/1) at 50 °C for 4 days. The macromers were prepared at two different molar ratios of MBA: AP: ALE, namely 1.1:0.9:0.1 and 1.1:0.7:0.3, which where denoted as MPAA1 and MPAA2, respectively. Typically, to prepare MPAA1 macromer, MBA (308 mg, 2 mmol), AP (171 mg, 1.66 mmol) and ALE (50 mg, 0.18 mmol) were dissolved in water/methanol mixture (v/v = 1/1, 9.6 mL in total) and stirred at 50 °C for 4 days under nitrogen. The solution was then diluted with water and dialyzed using a membrane with a molecular weight cut-off of 1000 in distilled water to remove the unreacted components. The product was obtained as a white solid after lyophilization. A control macromer without ALE, denoted by MAAc, was also synthesized from MBA and AP at 1.1:1 M ratio as described above. The yields of the products MAA1, MAA2, and MAAc were 60, 50, and 65%, respectively.

2.4. pH titration

PAA macromers, 50 mg of each macromer was dissolved in deionized water at a concentration of 1.0 mg/mL and the pH was adjusted to 2.0 using 2 M HCl solution. The macromer solution was titrated with 0.1 M NaOH with increments of 0.05 mL until pH 11.0. The increase in pH was recorded with a pH meter (WTW Inolab pH 720) at room temperature. The pK_b value was determined from the inflection point of the titration curve which responds to the pH value where 50% of protonated amine groups are neutralized.

2.5. Preparation of cryogels

0.1 g PAA macromer and the photoinitiator Irgacure 2959 (5 wt %) were dissolved in 0.9 mL distilled water and placed into glass vials

(diameter: 9 mm, thickness: 5 mm). The solutions were cooled to −18 °C and held at this temperature for 6–8 h. They were then exposed to UV light (365 nm, approximately 248 W/m^2) for 15 min in a photoreactor (Kerman UV/18, inner radius 15 cm, height 30 cm) containing 12 Philips TL 8 W BLB lamps on the perimeter. The cryogels were thawed at room temperature, lyophilized and weighed (W_i). Then, they were washed with ethanol and distilled water to remove unreacted macromers, dried under vacuum and weighed again (W_f). The percent gelation was calculated as,

$$Gelation(\%) = \frac{W_f}{W_i} \times 100 \quad (1)$$

2.6. Swelling studies

Dry cryogel samples were immersed in water, buffer solutions (pH 9, 7.4, 6.0, 2.0), and $CaCl_2$ (0.5 M) solution at 37 °C to reach equilibrium swelling. Then the samples were removed from the solutions, the excess solution was removed with a tissue paper and the swollen weight was measured. The degree of swelling (D_s) was calculated using

$$D_s = \frac{W_s - W_d}{W_d} \times 100 \quad (2)$$

where W_s and W_d refer to the weight of swollen and dry gel samples, respectively. The average data obtained from triplicate measurements were reported.

2.7. Degradation studies

Each lyophilized cryogel was weighed as W_i and then immersed in PBS (pH 7.4) at 37 °C. After incubation at 37 °C for 1, 2 and 4 weeks, the samples were taken out, rinsed with water, freeze-dried and re-weighed as W_f.

The degradation % was calculated according to

$$Degradation\ (\%) = \frac{W_i - W_f}{W_i} \times 100 \quad (3)$$

2.8. In vitro mineralization

2.8.1. Preparation of immersion solutions

Simulated Body Fluid (SBF) was prepared as described by Kokubo and Takadama [48].

A buffer solution (2 L, pH 7.4) containing 142 mM Na^+, 5 mM K^+, 1.5 mM Mg^{2+}, 2.5 mM Ca^{2+}, 147.8 mM Cl^-, 4.2 mM HCO_3^-, 1 mM HPO_4^{2-}, and 0.5 mM SO_4^{2-} was prepared in ultrapure water.

5 times concentrated SBF (5xSBF) was prepared as described by Chou et al. [49]. $CaCl_2$, $MgCl_2$, $NaHCO_3$ and $K_2HPO_4.3H_2O$ were dissolved in ultrapure water. Solution pH was lowered to 6 by adding 1 M HCl to increase the solubility. Then Na_2SO_4, KCl and NaCl were added until the solution become clear. The final pH was adjusted to 6.0 with 1 M HCl or 1 M NaOH. Both solutions were filter sterilized (Millipore, sterivex filter unit, 0.22 μm) and stored at +4 °C.

2.8.2. Mineralization of cryogel samples

Biomimetic mineralizations of cryogels were carried out by two different methods. In the first method, cryogel samples were immersed in 0.2 M $CaCl_2$ solution for one day, then washed with deionized water 3 times, then placed in 15 mL falcon tubes containing 10 mL of freshly prepared and filtered SBF solution, and incubated at 37 °C while shaking gently (50 rpm). The SBF was changed every two days. After 4 weeks the cryogel samples were taken out of the solution, rinsed with ultrapure water, and then freeze-dried to constant weight.

In the other method, to accelerate the biomineralization process from 4 weeks to 2 days, the cryogels were immersed in 10 mL of 5xSBF and incubated at 37 °C for two days, during which 5xSBF being changed every day. The cryogels were then taken out of the solution, rinsed with ultrapure water and then freeze-dried to constant weight. The characterization of mineralized hydrogels was carried out by using TGA, FTIR, SEM and XRD analyses.

2.9. Mechanical studies

Mechanical properties of cryogels in dry and equilibrium swollen states in water were investigated in a thermostated room at 23 ± 2 °C using uniaxial compression measurements on a Zwick Roell test machine with a 500 N load cell. The tests were carried out at a constant cross-head speed of 1 mm min^{-1}. The nominal σ_{nom} and true stresses σ_{true} ($= \lambda\sigma_{nom}$) were recorded, which are the forces acting per unit area of the undeformed and deformed gel specimens, respectively, and λ is the compression ratio. The strain was calculated as ε, the change in the length of the specimen with respect to its initial length, i.e., $\varepsilon = 1 - \lambda$. The compressive strength and strain at break of the cryogels were calculated from the maxima in σ_{true} versus ε curves as detailed before [50]. Young's modulus E of the cryogels was calculated from the slope of stress−strain curves between 5 and 10% compression.

2.10. In vitro cytotoxicity assay

Impact of the degradation products of prepared gels on the viability of Saos-2, U-2 OS and C2Cl2 cell lines was evaluated using the standart MTT assay. The Saos-2 and U-2 OS cells were cultured in McCoy and DMEM complete medium, respectively, supplemented with 10% (v/v) FBS and 1% (v/v) pen-strep in a 5% CO_2-humidified incubator at 37 °C and passaged every 2–3 days. C2C12 cells were cultured in the same way using phenol red free-DMEM. For viability test, 100 μl degradation product in cell culture medium was added to each well of a 96 Well-plate at a concentration between 12.5 and 200 μg/mL. Then, cells were seeded at a density of 15x10^3 cells in 100 μl DMEM complete medium in each well and incubated at 37 °C in 5% CO_2 atmosphere. After 48 h incubation, the cell viability was assessed using MTT colorimetric assay. First, 50 μl of MTT solution (5 mg/mL in PBS) was added into each well with 150 μL of culture medium and incubated for 4 h. Then, the purple formazan crystals formed as a result of mitochondrial activity in viable cells were dissolved with ethanol:DMSO (1:1 v/v) mixture. Absorbance at 570 nm with a reference reading at 630 nm was recorded for each well using a Synergy – H1 microplate reader (BioTek Instruments Inc., Winooski, VT, USA). Cells which were not exposed to degradation products of gels were used as controls. 100% viability is assumed for the control cells. The relative cell viability was calculated by

$$Cell\ viability\ (\%) = \frac{Absorbance_{sample}}{Absorbance_{control}} \text{x } 100 \quad (4)$$

2.11. Statistical analysis

Statistical analyses of the degradation products were conducted by using ordinary one-way ANOVA analysis of variance followed by multiple Dunnett's comparison test of GraphPad Prism 8.3.0 software package (GraphPad Software, Inc., USA). All measurements were expressed as mean values ± standard deviation (SD) based on 8, 7 and 5 replicas for U-2 OS, Saos-2 and C2C12 cells, respectively. Significance between different alendronate concentrations was conducted by using non-parametric Mann-Whitney test of GraphPad Prism 8 software. All results were two tailed. $p < 0.05$ was accepted as statistically significant difference.

3. Results and discussion

3.1. Synthesis and characterization of PAA macromers

Two novel bisphosphonic acid functionalized PAA macromers,

MPAA1 and MPAA2, were synthesized by aza-Michael reaction of MBA with AP and ALE at a fixed MBA:amines feed molar ratio of 1.1:1 (Fig. 1). AP serves as a hydrophilic diluent, as also used before in the preparation of many biomaterials, in particular for gene delivery applications [51]. We prepared PAA macromers at two different molar ratios of AP to ALE, namely 90:10 and 70:30 which are denoted as MPAA1 and MPAA2, respectively. The molar ratio of AP:ALE in macromers controls the bisphosphonic acid functionality and hence tunes the hydrophilicity, degradability, mineralization and mechanical properties of the resulting PAA cryogels. In the literature, PAAs are mainly prepared in methanol or methanol:water mixtures because these protic solvents facilitate the reaction by activating both the amine and the acrylate through hydrogen bonding [52,53]. Here, we used equivolume mixture of methanol and water as the solvent because while sodium alendronate is soluble only in water, and MBA is slightly soluble in water but soluble in methanol, the resulting macromers are only soluble in this mixture. The total concentration of the reactants was fixed at 0.4 M which was the maximum reachable concentration in the solvent. A control macromer denoted by MPAAc was also synthesized under the same conditions in the absence of ALE in order to investigate effect of bisphosphonic acid functionality on the cryogel properties. The macromers were obtained as white solids in 50–65% yields after dialysis. The composition and properties of macromers are summarized in Table 1.

The structures of the macromers were confirmed using ^{1}H NMR (Fig. 2, Fig. S1, Fig. S2) and FTIR (Fig. S3) spectroscopies. The peaks at 6.26 and 5.83 ppm indicate the end-capping acrylamide protons. The characteristic peaks of methylene protons of ALE appear at 1.42 (y), 1.69 (z), 3.04 (x) and 3.27 (f) ppm. The peaks at 1.33 (o), 1.50 (p), 1.57 (n), 3.59 (r) and 2.54 (m) are due to methylene protons of AP. The average number of ALE repeating units was calculated via comparison of the areas of the double bond protons (6 protons) to methylene protons of ALE at 1.69 ppm (2 protons). The double bond protons (6 protons) were also integrated with respect to methylene protons of AP at 1.57 or 3.59 ppm (2 protons) to find average number of AP repeating units. From the total number of ALE and AP repeating units and the formula weights of ALE and AP repeat units, and the formula weight of the end group (MBA), number-average molecular weights M_n of ALE-functionalized macromers MPAA1 and MPAA2 were calculated as 1365 and 1150 g/mol, respectively, which are lower than the control macromer MPAAc prepared without ALE, 1900 g/mol. Moreover, yield of gelation decreased with increasing ALE content of the macromers. These all suggest higher steric hindrance of ALE as compared to AP, decreasing both the molecular weight and macromer yield. Degree of ALE substitution to macromers were found as 8 and 15 mol % for MPAA1 and MPAA2, respectively. The FTIR spectra of the macromers show broad peaks in the region of 3500−3100 and 3000−2800 cm^{-1} due to OH and NH stretching and strong peaks at 1712 cm^{-1} due to C═O stretching. Moreover, the strong bands at 1070 and 1020 cm^{-1} correspond to the symmetric and asymmetric vibration of P–O. The thermal properties of the macromers investigated by DSC revealed that their glass transition temperatures (T_g) well-correlate with their chemical structures (Table 1). The ALE functionalized and hence bisphosphonic acid salt-containing macromers exhibit a higher T_g as compared to the reference macromer, MPAAc, and T_g increases with increasing amount of ALE, i.e., −1, 4 and 12 °C for 0, 10, and 30 mol % ALE, respectively, due to the presence of steric hindrance of bulky side group and polar interaction.

Table 1
Feed compositions during macromer synthesis, number average molecular weights (M_n) and T_g of the macromers.

Macromer	MBA (mol)	AP (mol)	ALE (mol)	Yield (%)	M_n[a] (g/mol)	T_g (°C)
MPAA1	1.1	0.9	0.1	60	1365	4
MPAA2	1.1	0.7	0.3	55	1150	12
MPAAc	1.1	1.0	0	65	1900	−1

[a] Calculated from ^{1}H NMR spectra.

PAAs are pH-responsive cationic polymers because of the tertiary amine functionality in their structures, i.e., the tertiary amines are unprotonated at a high pH (~9–10) and they become protonated at a low pH (~4). They have buffer capacity (usually defined as the percentage of amino groups that becomes protonated in the pH range 7.4 to 5.1) indicated by a relatively flat slope. The pH-responsiveness of the synthesized macromers was determined by titration method, results shown in Fig. 3a, which is typical of the pH sensitivities of poly(amido amine)s as seen in the literature [54,55].We found that the pH sensitivity of the present PAAs depends on the chemical structure and can be tuned by changing components such as MBA and amines used in the macromer preparation. For example, when the hydrophilic alendronate groups were introduced, the pK_b values shifted to higher regions (7.01, 7.22 and 7.39 for MPAAc, MPAA1 and MPAA2). A similar structure effect was also reported for poly(β-amino esters)in the literature [56]. It was observed that for the macromers with longer alkyl chains, a higher proton concentration was needed to protonate the tertiary amine chains, thus pK_b values were shifted to lower regions. The effect of macromer structure was more significant on the pH-responsiveness plateau. The wider plateau of MPAAc indicates its better pH-responsive performance, whereas MPAA2 with higher hydrophilicity does not show a distinct plateau region. This can be explained by continuous deprotonation of bisphosphonic acid groups in the alendronate with an increase in pH as given in Fig. 3b [57].

3.2. Synthesis and properties of cryogels

Cryogels were fabricated at a subzero temperature by free radical photopolymerization of aqueous 10 wt % macromer solutions. Because of the freezing of water in the reaction solution, the macromers and initiator are concentrated in the nonfrozen liquid microphase [13]. The gelation reactions thus occur in this unfrozen microphase surrounded by ice crystals acting as a template to produce the macroporous structure. As reported before, this technique allows fabrication of scaffolds with an interconnected macroporous structure. After around 15 min of the reaction, cryogels were thawed at room temperature and subsequently washed to remove unreacted macromeric precursors and the initiator. After drying, the gelation percentages were found to be in the range from 65% to 72%. The thermal properties of the cryogels were also studied using DSC. The glass transition temperatures T_g of the PAAc, PAA1 and PAA2 cryogels were found to be 37, 52 and 64 °C,

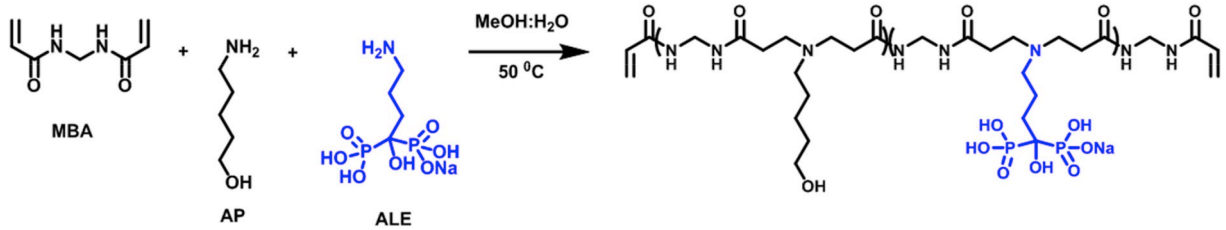

Fig. 1. Synthesis of PAA macromers.

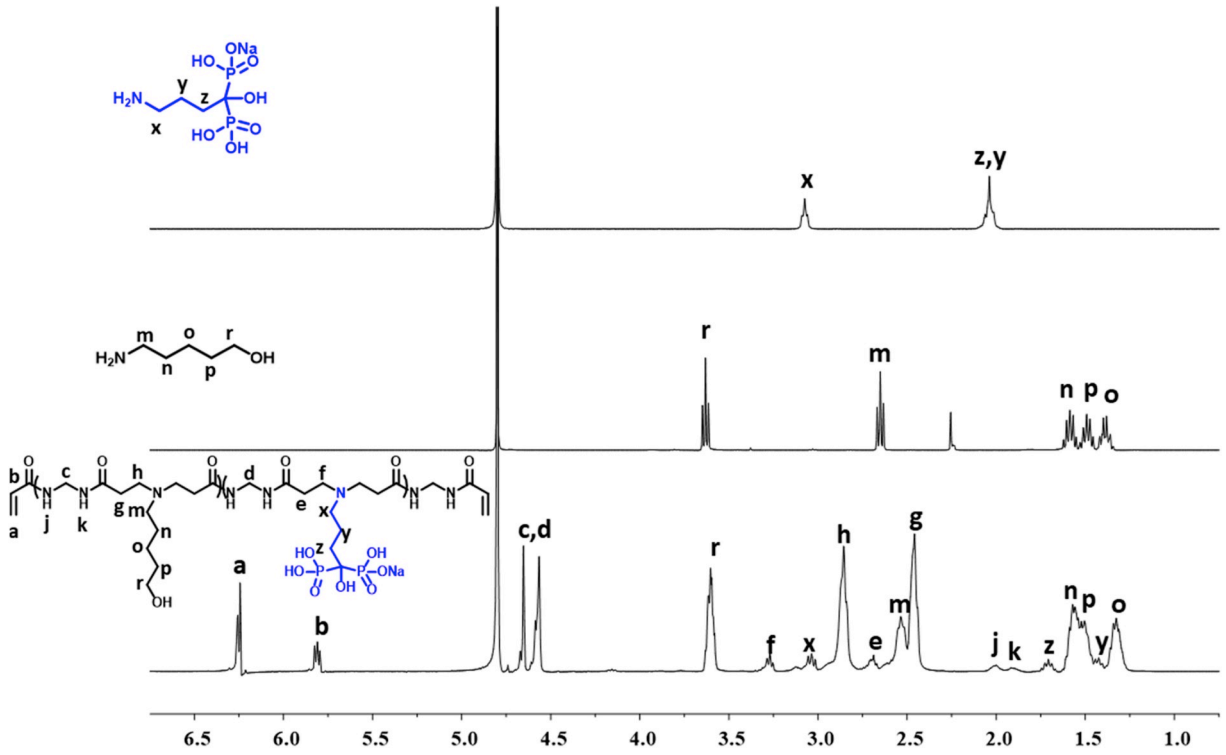

Fig. 2. ^{1}H NMR spectra of sodium alendronate, 5-amino-1-pentanol and MPAA1 macromer in D_2O.

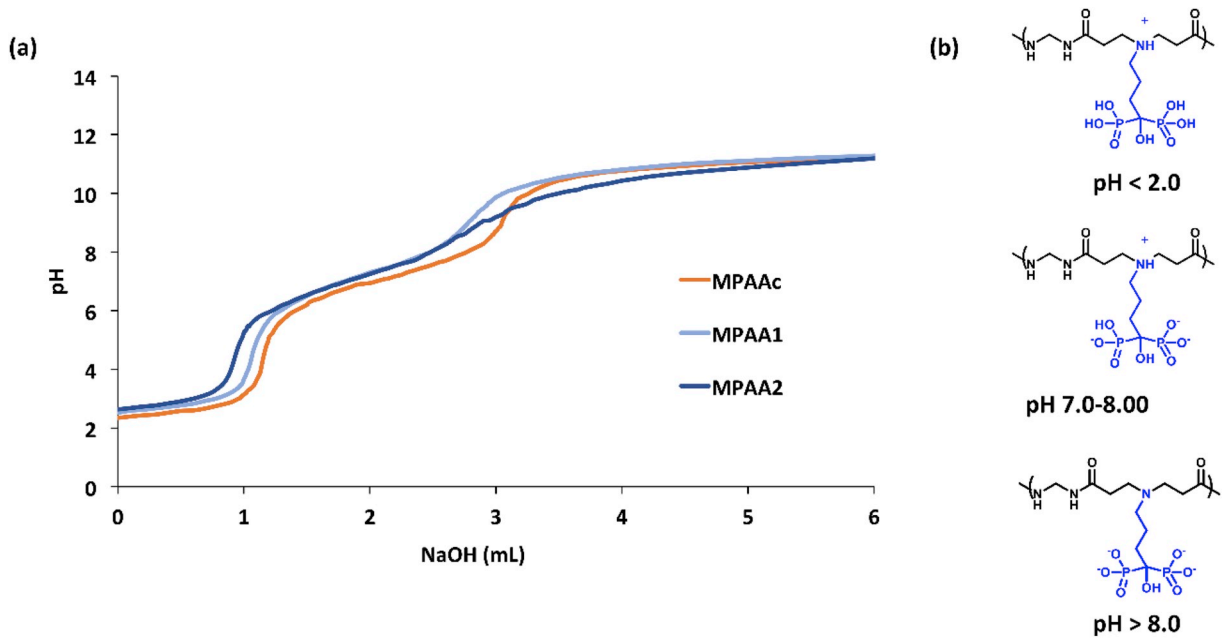

Fig. 3. (a) pH-responsive titration curves of MPAA1, MPAA2 and MPAAc in aqueous solutions and (b) structures of alendronate units in macromers at different pH.

respectively, well correlated with those of their macromers. There are many factors affecting properties of cryogels. The temperature at which cryogelation occurs, polymerization time, type of crosslinking, contents of monomers used, and freezing rate are variables determine physical properties of cryogels [13]. In our work most of the synthesis parameters (temperature, time rate of freezing, etc.) were constant, giving cryogels with similar pore sizes of 38, 44 and 43 μm for PAAc, PAA1 and PAA2, obtained from SEM images (Fig. S4); this qualifies them as supermacroporous.

3.3. Swelling studies

Cryogels were subjected to swelling measurements in distilled water, $CaCl_2$ solution (0.5 M) and different buffers with pH 2, pH 6, pH 7.4 and pH 9. For all cryogels, equilibrium swelling is reached very fast, within 5 min, as expected due to their macroporous structures facilitating the diffusion of water though the pores into the 3D cryogel network. Swelling percentages of the cryogels after 24 h (Fig. 4) show that the swelling percentages of cryogels are similar in water, pH 7.4 and pH 9; however, the swelling gets higher as the medium becomes more acidic.

At each pH and in $CaCl_2$, the swelling of PAA1 is highest.

The swelling is affected by both the molecular structure and molecular weight of the macromer precursors. The difference in the swelling behavior of the control cryogel (PAAc) and the others can be explained by hydrophilic/hydrophobic properties of the cryogels. Although the PAAc control has the highest molecular weight which leads to the lowest crosslink density, ALE containing PAA1 cryogel shows a higher water uptake because of its ionic bisphosphonic acid groups at the side chain of polymer backbone. The higher ionic strength in the cryogel can cause a higher degree of swelling of PAA1 cryogel than the non-ionic PAAc cryogel. Although MPAA2 possesses a higher amount of ALE at the backbone, its cryogels swelled less at pH 2 because the molecular weight of MPAA2 is lower than MPAA1 and MPAAc. The protonation of the amino groups creates positively charged groups, giving rise to stronger swelling. The lower swelling at higher ALE concentrations can be explained by a decrease in total charge due to the ALE functionality, whose effect is attracting the chains together electrostatically. As the pH increases ionization of four hydroxyl groups of ALE occurs, creating also negative charge density on the polymer, while deprotonation of amine groups decreases the positive charge on the polymer. The magnitude of the total charge of the hydrogel stays nearly the same for a comparatively wide range of pH, leading to almost constant swelling between pH 7 and 9. When the hydrogels were immersed in 0.5 M $CaCl_2$ solution, exchange of sodium ions with calcium is expected. The interaction between bisphosphonic acid groups and Ca^{2+} ions may form physical crosslinking. Therefore PAA2 gels with higher ALE content swelled less in $CaCl_2$ solution compared to PBS.

3.4. Degradation studies

The degradation behavior of the cryogels was investigated in PBS (pH 7.4) at 37 °C (Fig. 5a). The mass loss of the gels was found to change between 5 and 38% in four weeks, and it decreases as the molecular weight of the precursor macromer is decreased, the effect of which dominates over other possible effects of the chemical structure such as hydrophilicity coming from incorporation of sodium alendronate. For example, the mass loss of gels made from MPAAc was found to be 38% in 4 weeks whereas for MPAA1 and MPAA2 gels the respective weight losses were 30 and 14%. This might be explained by the higher number of hydrolytically susceptible linkages between the crosslinks for higher molecular weight macromers. During degradation in PBS, pore size of the gels increased significantly. For example, after 4 weeks in PBS, the pore size of PAA1 increased from 44 μm to 54 μm (Fig. 5b).

3.5. Mineralization

The synthesized cryogels were evaluated for their ability to mineralize apatite. It is expected that binding of Ca^{2+} to the ALE groups of the cryogels will lead to the initial nucleation for the mineralization of the cryogels. According to Hamai et al., Ca^{2+} incorporation into the polymer may accelerate apatite formation in SBF because of increase in Ca^{2+} release from the polymer [58]. Therefore, increasing ALE concentration of the cryogels may promote mineralization. The studies by Phadke et al. also showed that small changes in matrix interfacial hydrophobicity independent of functionality can profoundly influence the Ca^{2+} binding and formation of hydroxyapatite-like mineral phases on hydrogel matrices [59]. The synthesized cryogels were mineralized using two methods: (a) immersion in SBF, (b) immersion in 5xSBF. SBF was chosen because it closely mimics the ionic concentrations and pH typically observed in plasma [60]. Because the biomimetic mineralization occurs slowly, the experiments were also conducted at high SBF concentrations (5xSBF) in order to increase the rate of mineralization [61]. Before soaking in SBF for 4 weeks or 5xSBF for 2 days, the cryogels were immersed in 0.2 M $CaCl_2$ solution to exchange sodium with calcium. Mineralization of the cryogels was studied by using SEM, FTIR, XRD and TGA.

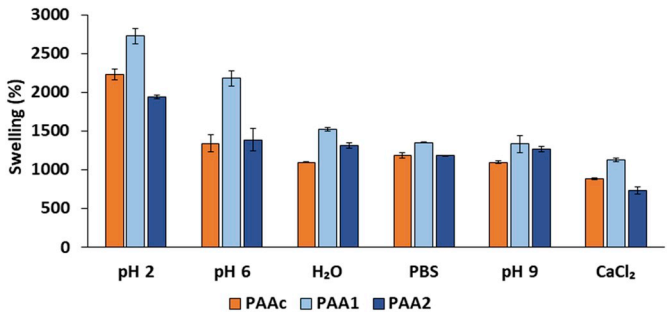

Fig. 4. Swelling percentages of PAA cryogels in water, buffer solutions (pH 7.4, 6.0, 2.0) and $CaCl_2$ (0.5 M) after 24 h. All the experiments were carried out in triplicates (n = 3) and mean average values with standard error (±SD) are represented in the error bars.

3.5.1. Characterization of mineralization using TGA

In order to observe the level of mineral deposition, we performed TGA measurements. The TGA thermograms of PAA2 cryogels before and after mineralization and the control cryogel before mineralization are shown in Fig. 6. They all show an initial weight loss starting from room temperature up to 100 °C due to removal of adsorbed water. The main weight loss occurred between ca. 250 and 400 °C due to degradation of the main chain. The PAA2 cryogel had higher residual weight (43%) than the control cryogel (18%) at 500 °C and above. The difference in the residual weight was due to ALE amount in the cryogel. In case of mineralized PAA2 cryogels the residual weights were highest (55%) due to the amount of deposited mineral. Additionally, the main weight loss was shifted to higher temperature (from ca. 230–254 °C) probably due to the higher thermal stability of the hybrid material.

3.5.2. Characterization of mineralization using FTIR and XRD

FTIR spectra of calcium phosphate materials are dominated by the two orthophosphate (P–O) absorption bands at 1130-1030 cm^{-1} and 600-560 cm^{-1}. In HAP, two major and one minor bands corresponding to phosphate were observed: 1016 (ν_3PO mode), 559, 600 (ν_4PO mode) and 964 cm^{-1} (ν_1PO mode) [62]. The FTIR spectra of the cryogels contained two broad peaks at around 1017–1050 and 530 (P–O) cm^{-1}. When the cryogels were mineralized, we observed an increase and slight shift in both bands and the appearance of a new band at 965 cm^{-1} which is related to the HAP spectrum (Fig. 6c). These changes become more clear with increase in alendronate concentration; PAA2 was found to mineralize faster compared to PAA1. Here, we suggest the formation of a calcium phosphate precursor such as dicalcium phosphate dehydrate (DCPD) within the cryogel which can hydrolyzes to apatite subsequently [63]. Surprisingly, the IR spectrum of mineralized PAAc was found to be similar to that of HAP. In the literature it was observed that not only polyanions, but also polycations such as lineer PEI have a strong influence on CaP mineralization [64]. LPEI accelerates the transformation brushite ($CaHPO_4$,$2H_2O$) (DCPD) to HAP by acting as a proton acceptor, which takes up the protons released from either the calcium phosphate precipitate during the phase transformation or from ions present in solution during a presumed, but so far not directly observed, dissolution–reprecipitation process [65]. XRD spectra of mineralized cryogels also indicated that the mineral grown via incubation in was apatitic (Fig. 6b), as seen from the peaks at 27 and 32° [66].

3.5.3. SEM studies

Although FTIR spectroscopy is a non-invasive technique for molecular characterization of the mineralized samples, it does not provide morphological information. Therefore we used SEM images to study the morphology of the minerals (Fig. 7). The freeze-dried cryogel samples were used for SEM analysis. The samples were opaque before mineralization and did not change their appearance after mineralization. SEM

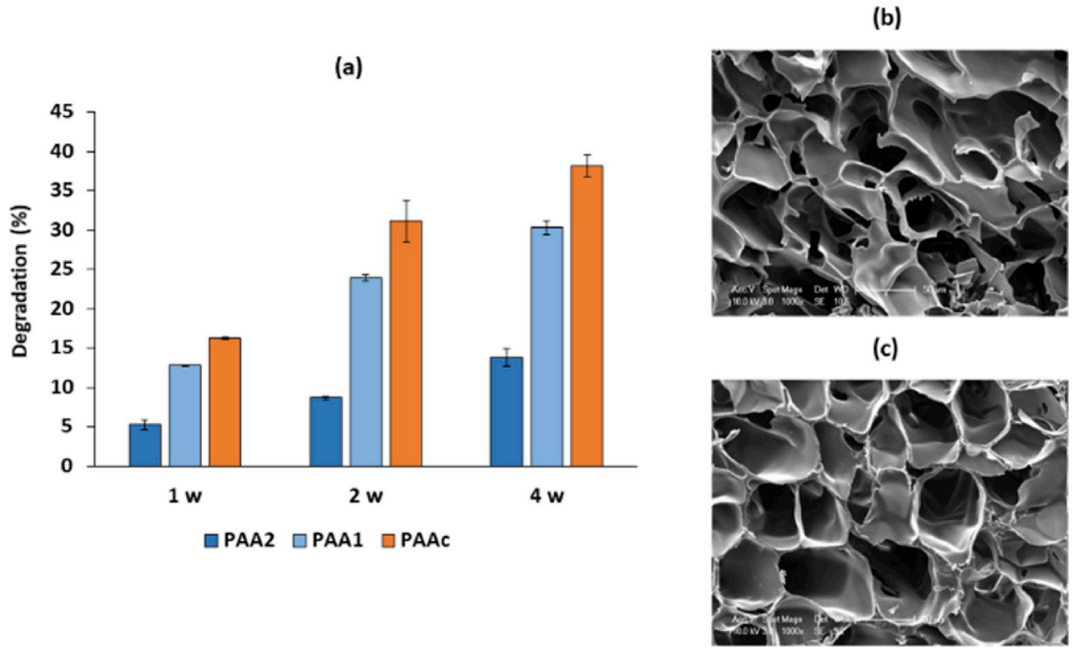

Fig. 5. (a) Degradation behaviour of cryogels in PBS (pH 7.4) at 37 °C, (b) SEM images of PAA1 cryogel before and (c) after 4 w degradation.

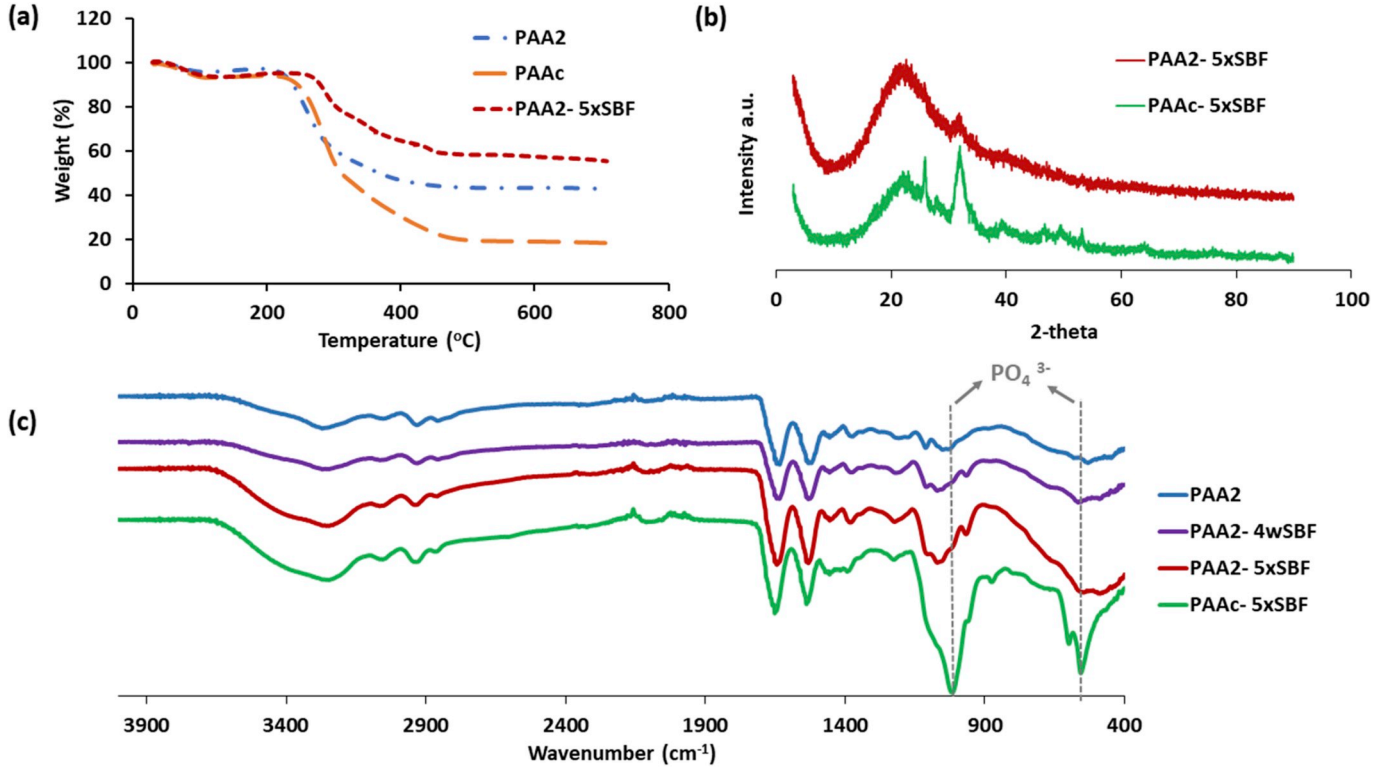

Fig. 6. (a) TGA thermograms of PAA2 (before and after mineralization in 5xSBF) and PAAc (before mineralization) cryogels, (b) XRD patterns of mineralized PAA2 and PAAc cryogels at 2 days in 5xSBF, (c) FTIR spectra of PAA2 (before and after mineralization in 5xSBF and SBF) and PAAc (in 5xSBF) cryogels.

images of PAA1 cryogels after 4 weeks of mineralization in SBF showed mineral layers (Fig. 7b). The amount of mineral deposited was more significant for PAA2 cryogels after 2 days of mineralization in 5xSBF (Fig. 7c). The control sample displayed platelike morphology (Fig. 7d).

3.6. Mechanical properties

The effect of BP content of the cryogels on their mechanical strength was investigated by uniaxial compression tests. Fig. 8a and b shows nominal stress (σ_{nom})–strain (ε) curves and the mechanical parameters of water-swollen cryogels, respectively. All cryogels without (PAAc) or with BP (PAA1 and PAA2) sustain up to around 97% strain without any crack development reflecting their high toughness under compression load. Increasing BP content also increases both Young's modulus E and compressive strength σ_f of the cryogels. For instance, the modulus E of the reference BP-free PAAc cryogel is 5 ± 1 kPa whereas it increases to

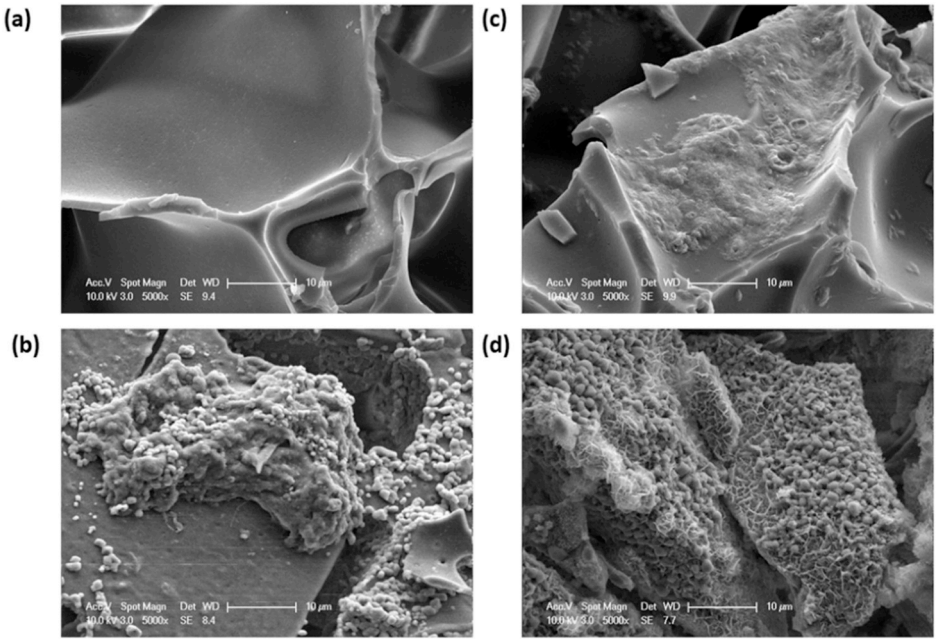

Fig. 7. SEM images of (a) PAA1 cryogel before mineralization, (b) PAA1 cryogel after 4 weeks of mineralization in SBF, (c) PAA2 cryogels after 2 days of mineralization in 5xSBF, (d) PAAc cryogel after 2 days of mineralization in 5xSBF.

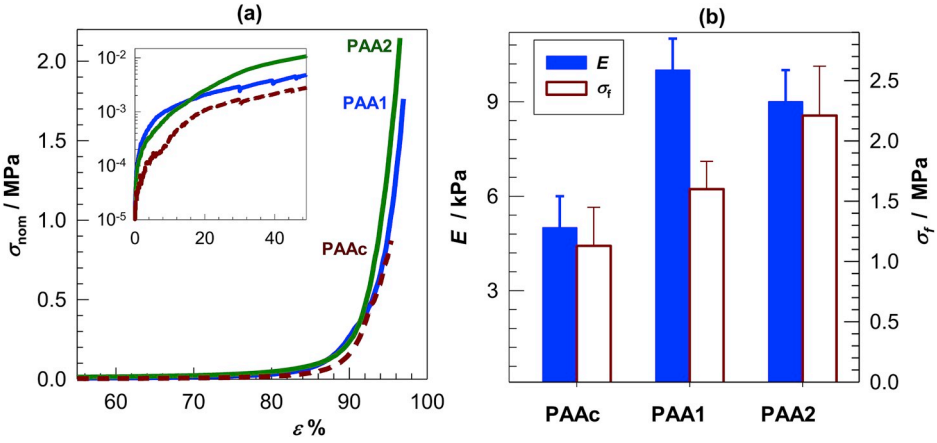

Fig. 8. Stress – strain curves (a) and the mechanical parameters E and σ_f (b) of PAAc, PAA1, and PAA2 cryogels swollen in water. The inset in (a) is zoom in to the data below 50% strain to highlight the initial mechanical properties.

10 ± 1 and 9 ± 1 kPa for ALE-functionalized PAA1 and PAA2 cryogels, respectively. Their compressive strengths σ_f are 1.1 ± 0.3, 1.6 ± 0.2, and 2.2 ± 0.4 MPa for PAAc, PAA1, and PAA2, respectively, revealing that σ_f increases in the order of PAAc < PAA1 < PAA2, i.e., in the order of increasing ALE content of the cryogels. Thus, the results show increasing stiffness and strength of the cryogels after their functionalization with ALE. The inset to Fig. 8a which is zoom in to the stress-strain data below 50% strain reveals the appearance of a plateau-like regime above 20% strain. Such a behavior was previously reported in silk fibroin cryogels and reflects squeezing out pore water from cryogels and hence, the plateau stress corresponds to the mechanical strength of the cryogel network [67,68]. Because the mechanical strength of the present cryogels increases after their functionalization with ALE, the plateau stress also increases with increasing ALE content (Fig. 8a). The mechanical tests were also conducted on dry cryogels (Fig. S5). Similar results were obtained except that both Young's modulus E and compressive strength σ_f attained much higher values. For instance, the modulus E of BP-free PAAc cryogel in dried state is 19 ± 8 kPa whereas it increases to 47 ± 7 and 327 ± 63 kPa for ALE functionalized PAA1 and PAA2 cryogels, respectively (Fig. S5). A similar trend was observed for the compressive strength σ_f of dried cryogels; σ_f was found to be 9.6 ± 0.6, 12 ± 2, and 11 ± 1 MPa for PAAc, PAA1 and PAA2 cryogels, respectively.

To highlight the effect of mineralization, mechanical tests were also conducted on cryogel specimens immersed in SBF and 5xSBF solutions corresponding to slow and fast mineralization procedures, respectively. The results are shown in Fig. 9a and b where the stress-strain curves and the mechanical parameters of the reference PAAc and ALE-functionalized cryogels PAA1 and PAA2 are presented. As expected, the mechanical properties of the reference PAAc hardly changed within the limits of experimental error after mineralization. However, mineralization significantly affects the mechanical performances of both ALE-functionalized cryogels. For instance, the modulus E of PAA2 cryogel increases from 9 ± 1 kPa to 41 ± 2 and 54 ± 21 kPa after mineralization in SBF and 5xSBF, respectively. The significant increase of the modulus indicates formation of additional cross-links within the cryogel network due to the binding of Ca^{2+} to the ALE groups and hence acting as cross-links. Indeed, similar results were obtained when cryogels were immersed in aqueous $CaCl_2$ solution (Fig. S6). The modulus E of ALE-

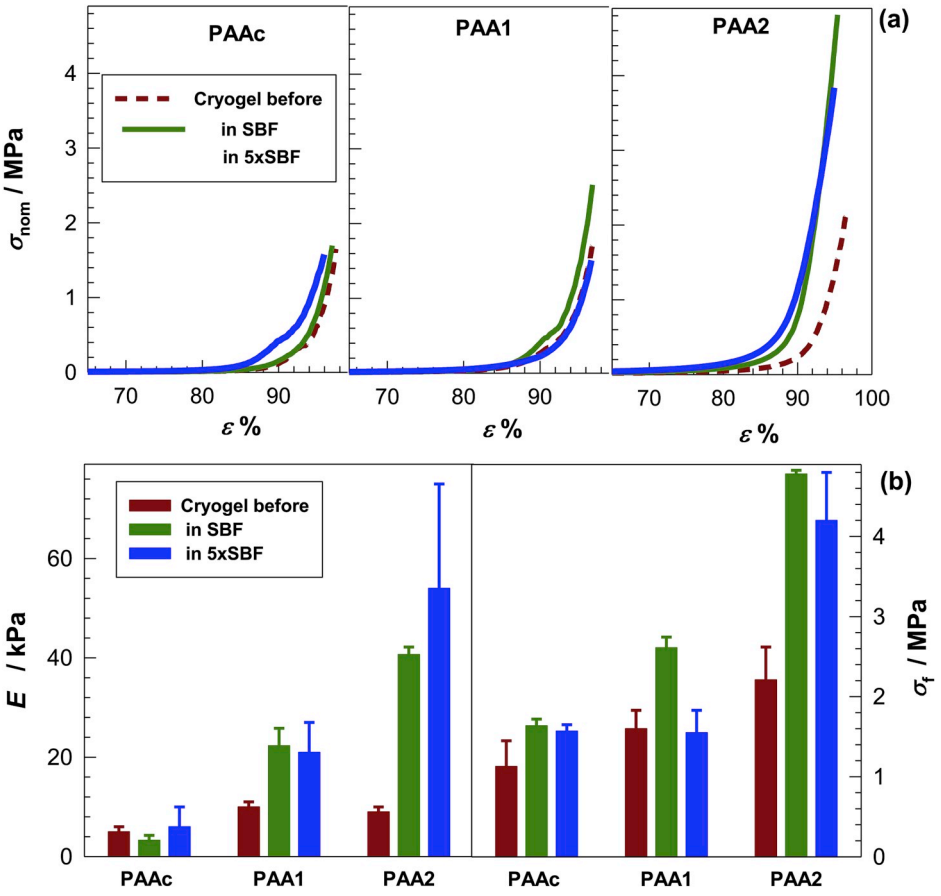

Fig. 9. Stress – strain curves (a) and the mechanical parameters E and σ_f (b) of PAAc, PAA1, and PAA2 cryogels before and after mineralization in SBF and 5xSBF.

functionalized PAA2 increases from 9 ± 1 to 25 ± 8 kPa in $CaCl_2$ solution reflecting formation of ionic cross-links. The compressive strength σ_f of the cryogels also increases after mineralization or in $CaCl_2$ solution but at much lesser extent (Figs. 9 and S6). For instance, σ_f of PAA2 cryogel is 2.2 ± 0.4 and 4.2 ± 0.6 MPa before and after mineralization in 5xSBF, respectively.

3.7. *In vitro cytotoxicity of cryogel degradation products*

Potential dose (12.5–100 μg/mL) dependent cytotoxicity of the PAA cryogel degradation products was evaluated on Saos-2, U-2 OS and C2Cl2 cells using the standard MTT assay, which indicates cell viability (Fig. 10). Cell viability above 80% is assumed as noncytotoxic according to ISO 10993–5 [69]. Since these cryogels have ALE in their composition, we also studied the influence of free ALE on the cell viability. PAAc lacks ALE and used as a control. Degradation products of PAAc did not reduce the viability of the cancer cell lines in a significant amount after 48 h exposure. Degradation products of PAA2, which has 30% ALE in its feed composition, reduced the viability of U-2 OS cells in a dose dependent manner in a greater extent compared to PAA1 with 10% ALE in the feed (Fig. 10a). Viability of U-2 OS was 77% at the lowest dose and then 66–68% for the rest of the doses in case of PAA2. This toxicity is mostly due to ALE component since PAAc did not exert any toxicity. Indeed, ALE caused a significant reduction in cell viability in all three cell lines. For example, viability of U-2 OS was 68% when treated with 100 μg/mL PAA2 and 44% when treated with 25 μg/mL free ALE. Viability of U-2 OS cells treated with PAA1 degradation products were all above 89% with no significant difference between doses due to lower content of ALE. ALE is not as toxic to SaOS-2 but still viability was dropped to 70–78% in the whole dose range. Parallel to this, viability of Saos-2 cells were above 90% when treated with PAA1 and significant reduction was observed with 50–100 μg/mL PAA2 degradation

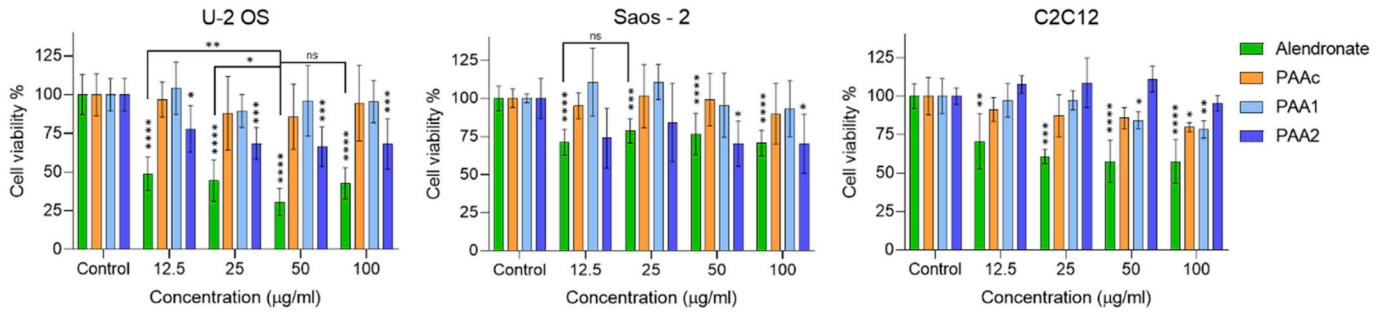

Fig. 10. Viability of U-2 OS, Saos-2 and C2C12 cell lines treated with Alendronate and degradation products of PAAc, PAA1 and PAA2 for 48 h. Viability was tested with MTT assay. Statistical significance: (*) $p < 0.0332$, (**) $p < 0.021$, (***) $p < 0.0002$, (****) $p < 0.0001$.

products. It was reported that ALE has an anti-invasive effect on some cancer cell lines including Saos-2 and U-2 OS [70]. This effect of bisphosphonates is usually attributed to inhibition of matrix metalloproteinases [70–72]. It was also reported that ALE induces apoptotic cell death, more in U-2 OS than Saos-2 in a study performed with 50–100 μM ALE with maximum cell death of 13.5% with 150 μM ALE after 48 h [70]. Concentration of ALE in our study is between 50 and 400 μM, hence reduction in cell viability that we observe as a function of ALE agrees with these reports.

Interestingly in C2C12, healthy muscle cells, 100 μg/mL PAAc degradation products reduced the viability to 80% and PAA1 showed more toxicity than PAA2 (78% versus 95% at 100 μg/mL) (Fig. 10c). Indeed, PAA2 treated cells were not different than control cells and PAA1 did not show significant difference from the control at the doses lower than 100 μg/mL. ALE reduced the viability from 76% to 57% in a dose dependent manner. It may be possible to say that PAAc component causes some toxicity in C2C12 cells while it was completely safe in the cancer cell lines in this study.

4. Conclusions

Two novel ALE and AP functionalized macromers with different compositions and a control macromer functionalized only with AP were synthesized and photopolymerized under cryogenic conditions to form cryogels to control the cryogel swelling, degradation, mechanical properties and their ability to support mineralization for biomedical applications. The swelling behavior of the cryogels is influenced both by molecular weight of the macromers and by the ion content determined by the ALE content and pH. The degradation percentages of the gels (5–38% in four weeks) are mostly affected by the molecular weight of the precursor macromer and overcome other possible effects of the chemical structure such as hydrophilicity coming from incorporation of sodium alendronate. The ALE functionalized cryogels have the ability *in vitro* growth of apatite, mostly DCPD and the extent of mineralization is influenced by the ALE content in the cryogel. Surprisingly the control cryogel, without ALE functionality, allows nucleation of HAP. Mechanical tests reveal that all cryogels are very tough and sustain up to around 97% compression without any crack development. The stiffness and strength of the cryogels increase after their functionalization with ALE groups. Both Young's modulus and compressive fracture stress of the cryogels increase with increasing ALE content and they attain maximum values of around 10 kPa and 2.2 ± 0.4 MPa, respectively. A significant increase in the modulus was also observed after mineralization of the cryogels in SBF due to the binding of Ca^{2+} to the ALE groups acting as physical cross-links. Safety of the degradation products seems to be dose, composition and cell type dependent. Most importantly, ALE between 12.5 and 100 μg/mL range reduces the viability of both U-2 OS and Saos-2 cancer cell lines and healthy C2C12 muscle cells and the major contributor to toxicity of cryogels seems to be the ALE component. However, degradation products of all cryogels are safe at 25 μg/mL and below. Above this dose, PAA2 with high ALE content is safe for C2C12 but toxic to cancer cells. Such cryogels may allocate toxic doses of ALE at the cancerous bone tissue and at the same time may provide new bone generation. Alternatively, cryogels with safe ALE content may be solely used for mineralization.Overall, these three PAA macromers and their cryogels have potential to be used as scaffolds for tissue engineering applications.

Declaration of competing interest

The authors declare that they have no known competing financial interests or personal relationships that could have appeared to influence the work reported in this paper.

CRediT authorship contribution statement

Melek Naz Guven: Investigation, Writing - original draft. **Gozde Demirci:** Investigation. **Seckin Altuncu:** Investigation. **Umit Gulyuz:** Investigation. **Oguz Okay:** Resources, Supervision, Writing - review & editing. **Havva Yagci Acar:** Resources, Supervision, Writing - review & editing. **Duygu Avci:** Conceptualization, Supervision, Writing - review & editing, Project administration.

Acknowledgments

This work was financed by TÜBITAK, Turkey grant number 117Z330.

Appendix A. Supplementary data

Supplementary data to this article can be found online at https://doi.org/10.1016/j.polymer.2020.122248.

References

[1] A.S. Hoffman, Hydrogels for biomedical applications, Adv. Drug Deliv. Rev. 64 (2012) 18–23.
[2] E. Caló, V.V. Khutoryanskiy, Biomedical applications of hydrogels: a review of patents and commercial products, Eur. Polym. J. 65 (2015) 252–267.
[3] C.C. Lin, K.S. Anseth, PEG hydrogels for the controlled release of biomolecules in regenerative medicine, Pharm. Res. 26 (2009) 631–643.
[4] P. Gupta, K. Vermani, S. Garg, Hydrogels: from controlled release to pH-responsive drug delivery, Drug Discov. Today 7 (2002) 569–579.
[5] C.H. Alarcon, S. Pennadam, C. Alexander, Stimuli responsive polymers for biomedical applications, Chem. Soc. Rev. 34 (2005) 276–285.
[6] M.A. Cohen Stuart, W.T.S. Huck, J. Genzer, M. Müller, C. Ober, M. Stamm, G. B. Sukhorukov, I. Szleifer, V.V. Tsukruk, M. Urban, F. Winnik, S. Zauscher, I. Luzinov, S. Minko, Emerging applications of stimuli-responsive polymer materials, Nat. Mater. 9 (2010) 101–113.
[7] D. Roy, J.N. Cambre, B.S. Sumerlin, Future perspectives and recent advances in stimuli-responsive materials, Prog. Polym. Sci. 35 (2010) 278–301.
[8] O. Okay, V.I. Lozinsky, Synthesis and structure–property relationships of cryogels, Polym. Cryogels 263 (2014) 103–157.
[9] A. Memic, T. Colombani, L.J. Eggermont, M. Rezaeeyazdi, J. Steingold, Z.J. Rogers, K.J. Navare, H.S. Mohammed, S.A. Bencherif, Latest advances in cryogel technology for biomedical applications, Adv. Ther. 2 (2019) 1800114.
[10] V.I. Lozinsky, Polymeric cryogels as a new family of macroporous and supermacroporous materials for biotechnological purposes, Russ. Chem. Bull., Int. Ed. 57 (5) (2008) 996–1013.
[11] T. Dispinar, W.V. Camp, L.J. De Cock, B.G. De Geest, F.E. Du Prez, Redox-responsive degradable PEG cryogels as potential cell scaffolds in tissue engineering, Macromol. Biosci. 12 (2012) 383–394.
[12] Y. Hwang, N. Sangaj, S. Varghese, Interconnected macroporous poly(ethylene glycol) cryogels as a cell scaffold for cartilage tissue engineering, Tissue Eng. 16 (2010) 3033–3041.
[13] M. Bakhshpour, N. Idil, I. Perçin, A. Denizli, Biomedical applications of polymeric cryogels, Appl. Sci. 9 (2019) 553.
[14] V.I. Lozinsky, I.Y. Galaev, F.M. Plieva, I.N. Savina, H. Jungvid, B. Mattiasson, Polymeric cryogels as promising materials of biotechnological interest, Trends Biotechnol. 21 (2003) 445–451.
[15] P. Ferruti, Poly(amidoamine)s: past, present, and perspectives, J. Polym. Sci., Polym. Chem. Ed. 51 (2013) 2319–2353.
[16] W. Cheng, D. Wu, Y. Liu, Michael addition polymerization of trifunctional amine and acrylic monomer: a versatile platform for development of biomaterials, Biomacromolecules 17 (2016) 3115–3126.
[17] P. Ferruti, M.A. Marchisio, R. Duncan, Poly(amido-amine)s: biomedical applications, Macromol. Rapid Commun. 23 (2002) 332–355.
[18] E. Jacchetti, E. Emilitri, S. Rodighiero, M. Indrieri, A. Gianfelice, C. Lenardi, A. Podestà, E. Ranucci, P. Ferruti, P. Milani, Biomimetic poly (amidoamine) hydrogels as synthetic materials for cell culture, J. Nanobiotechnol. 6 (2008) 14.
[19] P. Ferruti, S. Bianchi, E. Ranucci, Novel agmatine-containing poly(amidoamine) hydrogels as scaffolds for tissue engineering, Biomacromolecules 6 (2005) 2229–2235.
[20] F. Tocchio, F. Martello, M. Tamplenizza, E. Rossi, I. Gerges, P. Milani, C. Lenardi, RGD-mimetic poly(amidoamine) hydrogel for the fabrication of complex cell-laden micro constructs, Acta Biomater. 18 (2015) 144–154.
[21] V. Magnaghi, V. Conte, P. Procacci, G. Pivato, P. Cortese, E. Cavalli, G. Pajardi, E. Ranucci, F. Fenili, A. Manfredi, P. Ferruti, Biological performance of a novel biodegradable polyamidoamine hydrogel as guide for peripheral nerve regeneration, J. Biomed. Mater. Res. 98 (2011) 19–30.
[22] L. Yu, K. Xu, L. Ge, W. Wan, A. Darabi, M. Xing, W. Zhong, Cytocompatible, photoreversible, and self-healing hydrogels for regulating bone marrow stromal cell differentiation, Macromol. Biosci. 16 (2016) 1381–1390.

[23] P. Ferruti, S. Bianchi, E. Ranucci, F. Chiellini, V. Caruso, Novel poly(amido-amine)-based hydrogels as scaffolds for tissue engineering, Macromol. Biosci. 5 (2005) 613–622.
[24] F. Martello, A. Tocchio, M. Tamplenizza, I. Gerges, V. Pistis, R. Recenti, M. Bortolin, M. Del Fabbro, S. Argentiere, P. Milani, C. Lenardi, Poly(amido-amine)-based hydrogels with tailored mechanical properties and degradation rates for tissue engineering, Acta Biomater. 10 (2014) 1206–1215.
[25] S. Chen, J. Shi, X. Xu, J. Ding, W. Zhong, L. Zhang, M. Xing, L. Zhang, Study of stiffness effects of poly(amidoamine)–poly(n-isopropyl acrylamide) hydrogel on wound healing, Colloids Surf. B Biointerfaces 140 (2016) 574–582.
[26] J. Shi, J. Ouyang, Q. Li, L. Wang, J. Wu, W. Zhong, M.M.Q. Xing, Cell-compatible hydrogels based on a multifunctional crosslinker with tunable stiffness for tissue engineering, J. Mater. Chem. 22 (2012) 23952–23962.
[27] B. Peng, X. Lai, L. Chen, X. Lin, C. Sun, L. Liu, S. Qi, Y. Chen, K.W. Leong, Scarless wound closure by a mussel-inspired poly(amidoamine) tissue adhesive with tunable degradability, ACS Omega 2 (2017) 6053–6062.
[28] K. Gkioni, S.C.G. Leeuwenburgh, T.E.L. Douglas, A.G. Mikos, J.A. Jansen, Mineralization of hydrogels for bone regeneration, Tissue Eng. B Rev. 16 (2010) 577–585.
[29] G.S. Sailaja, P. Ramesh, S. Vellappally, S. Anil, H.K. Varma, Biomimetic approaches with smart interfaces for bone regeneration, J. Biomed. Sci. 23 (2016) 77.
[30] T.V. Chirila, Zainuddin, Calcification of synthetic polymers functionalized with negatively ionizable groups: a critical review, React. Funct. Polym. 67 (2007) 165–172.
[31] B.V. Slaughter, S.S. Khurshid, O.Z. Fisher, A. Khademhosseini, N.A. Peppas, Hydrogels in regenerative medicine, Adv. Mater. 21 (2009) 3307–3329.
[32] A.J. Salgado, O.P. Coutinho, R.L. Reis, Bone tissue engineering: state of the art and future trends, Macromol. Biosci. 4 (2004) 743–765.
[33] G. Boivin, P.J. Meunier, Effects of bisphosphonates on matrix mineralization, J. Musculoskel Neuron. 2 (6) (2002) 538–543.
[34] J.P. Cattalini, A.R. Boccaccini, S. Lucangioli, V. Mourino, Bisphosphonate-based strategies for bone tissue engineering and orthopedic implants, Tissue Eng. Part B 18 (2005) 323–340.
[35] X. Yang, S. Akhtar, S. Rubino, K. Leifer, J. Hilborn, D. Ossipov, Direct ″click″ synthesis of hybrid bisphosphonate−hyaluronic acid hydrogel in aqueous solution for biomineralization, Chem. Mater. 24 (2012) 1690–1697.
[36] S. Kootala, Y. Zhang, S. Ghalib, V. Tolmachev, J. Hilborn, D. Ossipov, Control of growth factor binding and release in bisphosphonate functionalized hydrogels guides rapid differentiation of precursor cells in vitro, Biomater. Sci. 4 (2016) 250–254.
[37] G. Hulsart-Billström, P. Kwan Yuen, R. Marsell, J. Hilborn, S. Larsson, D. Ossipov, Bisphosphonate-linked hyaluronic acid hydrogel sequesters and enzymatically releases active bone morphogenetic protein-2 for induction of osteogenic differentiation, Biomacromolecules 14 (2013) 3055–3063.
[38] Z. Yi, Y. Zhang, S. Kootala, J. Hilborn, D. Ossipov, Hydrogel patterning by diffusion through the matrix and subsequent light-triggered chemical immobilization, ACS Appl. Energy Mater. Interfaces 7 (2015) 1194–1206.
[39] M.R. Nejadnik, X. Yang, M. Bongio, H.S. Alghamdi, J.J.J.P. van den Beucken, M. C. Huysmans, J.A. Jansen, J. Hilborn, D. Ossipov, S.C.G. Leeuwenburgh, Self-healing hybrid nanocomposites consisting of bisphosphonated hyaluronan and calcium phosphate nanoparticles, Biomaterials 35 (2014) 6918–6929.
[40] M. Diba, J. An, S. Schmidt, M. Hembury, D. Ossipov, A.R. Boccaccini, S.C. G. Leeuwenburgh, Exploiting bisphosphonate bioactive-glass interactions for the development of self-healing and bioactive composite hydrogels, Macromol. Rapid Commun. 37 (2016) 1952–1959.
[41] M. Diba, W.A. Camargo, M. Brindisi, K. Farbod, A. Klymov, S. Schmidt, M. J. Harrington, L. Draghi, A.R. Boccaccini, J.A. Jansen, J.J.J.P. van den Beucken, S. C.G. Leeuwenburgh, Composite colloidal gels made of bisphosphonate functionalized gelatin and bioactive glass particles for regeneration of osteoporotic bone defects, Adv. Funct. Mater. 27 (2017) 1703438.
[42] M.N. Guven, M.S. Altuncu, T. Bal, D.C. Oran, U. Gulyuz, S. Kizilel, O. Okay, D. Avci, Bisphosphonic acid-functionalized cross-linkers to tailor hydrogel properties for biomedical applications, ACS Omega 3 (2018) 8638–8647.
[43] R.E. Dey, I. Wimpenny, J.E. Gough, D.C. Watts, P.M. Budd, Poly(vinylphosphonic acid-co-acrylic acid) hydrogels: the effect of copolymer composition on osteoblast adhesion and proliferation, J. Biomed. Mater. Res. 106A (2018) 255–264.
[44] C.R. Nuttelman, D.S.W. Benoit, M.C. Tripodi, K.S. Anseth, The effect of ethylene glycol methacrylate phosphate in PEG hydrogels on mineralization and viability of encapsulated hMSCs, Biomaterials 27 (2006) 1377–1386.
[45] B.A. Aderibigbe, E.R. Sadiku, S.S. Ray, X.Y. Mbianda, M.C. Fotsing, S.C. Agwuncha, S.J. Owonubi, Synthesis and characterization of polyamidoamine conjugates of neridronic acid, Polym. Bull. 72 (2015) 417–439.
[46] B.A. Aderibigbe, E.R. Sadiku, S.S. Ray, X.Y. Mbianda, M.C. Fotsing, S.J. Owonubi, S.C. Agwuncha, Synthesis, characterization and the release kinetics of antiproliferative agents from polyamidoamine conjugates, J. Microencapsul. 32 (5) (2015) 432–442.
[47] M. Casolaro, I. Casolaro, A. Spreafico, C. Capperucci, B. Frediani, R. Marcolongo, N. Margiotta, R. Ostuni, R. Mendichi, F. Samperi, T. Ishii, Y. Ito, Novel therapeutic agents for bone resorption. Part 1. Synthesis and protonation thermodynamics of poly(amido-amine)s containing bis-phosphonate residues, Biomacromolecules 7 (2006) 3417–3427.
[48] T. Kokubo, H. Takadama, How useful is SBF in predicting in vivo bone bioactivity? Biomaterials 27 (15) (2006) 2907–2915.
[49] Y.F. Chou, W.A. Chiou, Y. Xu, J.C.Y. Dunn, B.M. Wu, The effect of pH on the structural evolution of accelerated biomimetic apatite, Biomaterials 25 (2004) 5323–5331.
[50] A. Argun, V. Can, U. Altun, O. Okay, Nonionic double and triple network hydrogels of high mechanical strength, Macromolecules 47 (2014) 6430–6440.
[51] J.C. Sunshine, M.I. Akanda, D. Li, K.L. Kozielski, J.J. Green, Effects of base polymer hydrophobicity and end-group modification on polymeric gene delivery, Biomacromolecules 12 (2011) 3592–3600.
[52] E. Manfredi, E. Ranucci, M. Suardi, P. Ferruti, Polymerization kinetics of poly (amidoamine)s in different solvents, J. Bioact. Compat Polym. 22 (2007) 219–231.
[53] R. Wang, L. Zhou, Y. Zhou, G. Li, X. Zhu, H. Gu, X. Jiang, H. Li, J. Wu, L. He, X. Guo, B. Zhu, D. Yan, Synthesis and gene delivery of poly(amido amine)s with different branched architecture, Biomacromolecules 11 (2010) 489–495.
[54] M.A. Mateos-Timoneda, M.C. Lok, W.E. Hennink, J. Feijen, J.F.J. Engbersen, Poly (amido amine)s as gene delivery vectors: effects of quaternary nicotinamide moieties in the side chains, ChemMedChem 3 (2008) 478–486.
[55] C. Lin, J.F.J. Engbersen, PEGylated bioreducible poly(amido amine)s for non-viral gene delivery, Mater. Sci. Eng. C 31 (2011) 1330–1337.
[56] W. Song, Z. Tang, M. Li, S. Lv, H. Yu, L. Ma, X. Zhuang, Y. Huang, X. Chen, Tunable pH-sensitive poly(β-amino ester)s synthesized from primary amines and diacrylates for intracellular drug delivery, Macromol. Biosci. 12 (2012) 1375–1383.
[57] J. Ke, H. Dou, X. Zhang, D.S. Uhagaze, X. Ding, Y. Dong, Determination of pKa values of alendronate sodium in aqueous solution by piecewise linear regression based on acid-base potentiometric titration, J. Pharm. Anal. 6 (2016) 404–409.
[58] R. Hamai, Y. Shirosaki, T. Miyazaki, Apatite-forming ability of vinylphosphonic acid-based copolymer in simulated body fluid: effects of phosphate group content, J. Mater. Sci. Mater. Med. 27 (2016) 152.
[59] A. Phadke, C. Zhang, Y.S. Hwang, K. Vecchio, S. Varghese, Templated mineralization of synthetic hydrogels for bone-like composite materials: role of matrix hydrophobicity, Biomacromolecules 11 (2010) 2060–2068.
[60] A. Oyane, H.M. Kim, T. Furuya, T. Kokubo, T. Miyazaki, T.J. Nakamura, Preparation and assessment of revised simulated body fluids, Biomed. Mater. Res. 65A (2003) 188–195.
[61] D.O. Costa, B.A. Allo, R. Klassen, J.L. Hutter, S.J. Dixon, A.S. Rizkalla, Control of surface topography in biomimetic calcium phosphate coatings, Langmuir 28 (8) (2012) 3871–3880.
[62] G.R. Sauer, R.E. Wuthier, Fourier transform infrared characterization of mineral phases formed during induction of mineralization by collagenase-released matrix vesicles in vitro, J. Biol. Chem. 263 (1988) 13718–13724.
[63] J.L. Harding, M.D. Krebs, Controlled and tunable biomimetic apatite mineralization of synthetic hydrogels, Macromol. Mater. Eng. 301 (2016) 1172–1180.
[64] A. Shkilnyy, A. Friedrich, B. Tiersch, S. Schöne, M. Fechner, J. Koetz, C. W. Schlapfer, A. Taubert, Poly(ethylene imine)-controlled calcium phosphate mineralization, Langmuir 24 (2008) 2102–2109.
[65] A. Shkilnyy, S. Schöne, C. Rumplasch, A. Uhlmann, A. Hedderich, C. Günter, A. Taubert, Calcium phosphate mineralization with linear poly(ethylene imine): a time-resolved study, Colloid Polym. Sci. 289 (2011) 881–888.
[66] Y. Li, X. Chen, A. Fok, J.C. Rodriguez-Cabello, C. Aparicio, Biomimetic mineralization of recombinamer-based hydrogels toward controlled morphologies and high mineral density, ACS Appl. Mater. Interfaces 7 (2015) 25784–25792.
[67] F. Ak, Z. Oztoprak, I. Karakutuk, O. Okay, Macroporous silk fibroin cryogels, Biomacromolecules 14 (2013) 719–727.
[68] B. Yetiskin, O. Okay, High-strength and self-recoverable silk fibroin cryogels with anisotropic swelling and mechanical properties, Int. J. Biol. Macromol. 122 (2019) 1279–1289.
[69] R.F. Wallin, A Practical Guide to ISO 10993-5: Cytotoxicity, 1998.
[70] Y.Y. Cheng, L. Huang, K.M. Lee, S.M. Kumta, Alendronate regulates cell invasion and MMP-2 secretion in human osteosarcoma cell lines, Pediatr. Blood Canc. 42 (2004) 410–415.
[71] S. Muller, E. Migianu, M. Lecouvey, M. Kraemer, O. Oudar, Alendronate inhibits proliferation and invasion of human epidermoid carcinoma cells in vitro, Anticancer Res. 25 (2005) 2655–2660.
[72] Z.F. Xin, Y.K. Kim, S.T. Jung, Risendronate inhibits human osteosarcoma cell invasion, J. Exp. Clin. Canc. Res. 28 (2009) 105.